SINGLE CRYSTAL TURBINE BLADE INSPECTION USING A 2D ULTRASONIC ARRAY

C. J. L. Lane[1, 2] and A. K. Dunhill[1]
[1]Rolls-Royce plc, Bristol, UK
[2]Department of Mechanical Engineering, University of Bristol, UK

Abstract

In this paper a non-destructive method for inspecting jet-engine turbine blades for root cracking is developed. This method utilises 2D ultrasonic arrays to enable the detection and characterisation of sub-surface cracks in three-dimensions. The majority of modern turbine blades are manufactured from single crystals of nickel based superalloys which exhibit high elastic anisotropy. This complicates the inspection due to the complex behaviour of ultrasonic wave propagation in anisotropic media and the variation of the crystal orientation in turbine blades. This paper, therefore, addresses these issues to develop a reliable inspection for a typical jet-engine single crystal turbine blade.

Introduction

Turbine blades are the components within gas-turbine engines that exact mechanical power from the hot, high-pressure combustion gases. During operation these components are highly stressed, due to the aerodynamic and centrifugal loadings that act upon them, and are surrounded by gases that may exceed the incipient melting temperature of the bulk blade material. It is therefore desirable to have a sensitive non-destructive evaluation method to inspect these components to ensure safe operation under these extreme conditions.

2D ultrasonic phased arrays are one method which would potentially enable the volumetric inspection of turbine blades for accurate detection and characterisation of sub-surface defects[(1)]. Ultrasonic array systems are also portable enough to allow in-situ inspections, which removes the costly and time consuming process of stripping the turbine blades from the engine. However, modern turbine blades are cast from single crystals of nickel based superalloys for the excellent mechanical properties these materials exhibit at elevated temperatures[(2)]. Single crystal materials are elastically anisotropic which causes difficulties when inspection these materials with ultrasound, in particular causing a significant defocusing of the images produced by the phased array.

Recently the anisotropic propagation of ultrasound in single crystals has been modelled and these models were used to correct a volumetric imaging algorithm [(3)]. In this current paper the corrected algorithm is presented and is then applied to the inspection of cracking in a single crystal turbine blade.

Bulk Wave Propagation in Anisotropic Media

The phenomenon of anisotropic wave propagation has been discussed extensively in the literature, and is therefore only briefly presented here. A thorough discussion and derivation of governing equations can be found in Musgrave[(4)] and Červený[(5)]. For a more concise overview of the subject consult Rose[(6)] or Auld[(7)].

The most important aspect of wave propagation in anisotropic media for ultrasonic array inspection is that waves propagate with different velocity depending on the direction. This effect can be illustrated by referring to Figure 1. This figure shows images from finite element simulations that modelled waves propagating from a cylindrical point-source in isotropic and anisotropic media. In the isotropic case,

Figure 1 a, the individual longitudinal and slower shear wave modes propagate with a constant velocity in all directions and hence have a circular wave surface. The waves in the anisotropic case, Figure 1 b, propagate with different velocities depending on the direction and therefore the wave surface is non-circular.

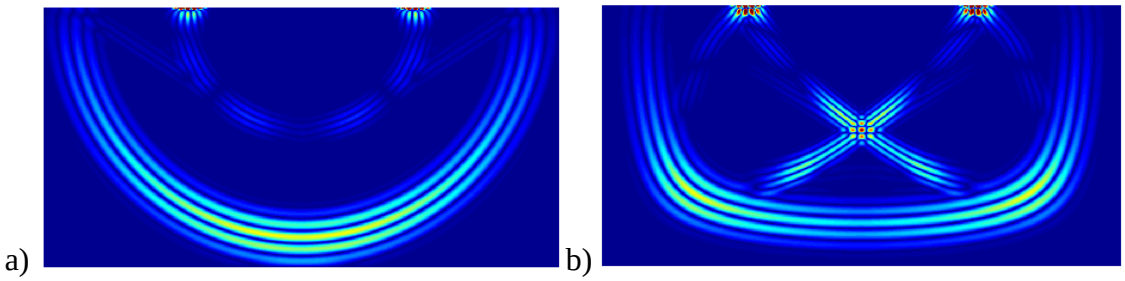

Figure 1. FE models of waves propagating in an elastic half-space from a point-source in a) an isotropic media and b) an anisotropic media.

Analytical models of the bulk velocities in anisotropic media have been developed and validated in a previous paper[3]. These models have been applied to CMSX-4 a single crystal nickel alloy widely used in the aerospace industry for turbine blades manufacture. Figure 2 shows the bulk longitudinal velocity profile in all directions in a sample of CMSX-4. The profile is shown as a spherical plot where the colour represents the different velocities. The model shows the profile varies from a minimum of 5194 m/s in the <001> crystallographic directions to a maximum of 6316 m/s relating to the <111> directions

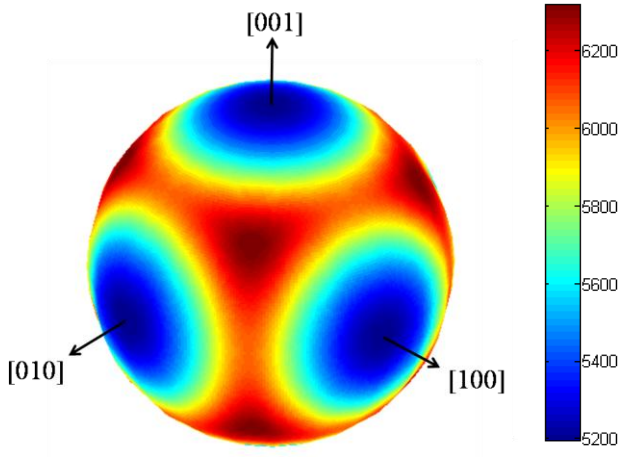

Figure 2. The bulk longitudinal group velocity profile of CMSX-4. Velocities are shown in m/s.

Corrected Ultrasonic Array Imaging

Ultrasonic array imaging techniques require signals from individual reflectors to be summed in phase to produce focused images with a high signal to noise ratio (SNR). To achieve this, the ray path between reflectors and array elements and the velocity along the ray paths must be known. If the directional dependence of the wave velocity in anisotropic materials is not accounted for in the imaging algorithm, the signals from a reflector will not be coherent leading to a defocusing of the resulting image.

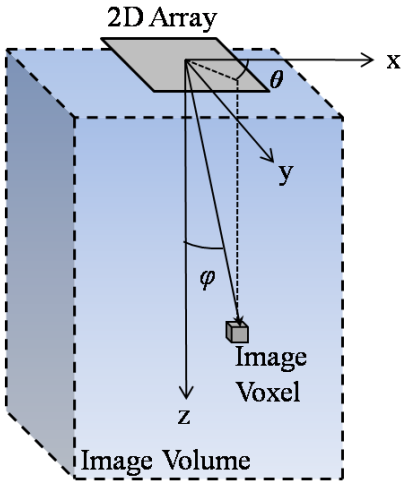

Figure 3. Ultrasonic array imaging geometry.

The 3D Total-Focusing Method (TFM)[8] algorithm is used in this work as it offers a high SNR, sensitivity and resolution. The TFM algorithm post-processes the full matrix capture (FMC) data from an ultrasonic array to synthetically focus ultrasonic energy at every location in the imaging field. The FMC data is collected by firing one array element and receiving on all others. This is performed for every transmit-receive combination to collect the full matrix.

Considering the volumetric imaging geometry shown in Figure 3**,** the TFM algorithm computes the intensity of a voxel in the imaging field, *I(x,y,z)*, by coherently summing the FMC data, $S_{ij,}$ with appropriate time delays to focus at that location. This can be represented mathematically as:

$$I(x,y,z) = \sum_{i=1,\,j=1}^{n} S_{ij}\left(t_{ij}(x,y,z)\right) \qquad 1$$

where n is the number of array elements and subscripts i and j indicate the transmit and receive elements respectively. The time of flight, t, of the ultrasonic pulse from the transmit element to the field point and back to the receive element is given by:

$$t_{ij}(x,y,z) = \frac{d_{i}(x,y,z)}{c_g\left(\vartheta_i(x,y,z),\varphi_i(x,y,z)\right)} + \frac{d_{j}(x,y,z)}{c_g\left(\vartheta_j(x,y,z),\varphi_j(x,y,z)\right)} \qquad 2$$

where c_g is the velocity profile defined using spherical coordinates, φ and θ, and $d_{i,j}$ is the ray path distances between the image voxel and array elements which is computed as:

$$d_{i,j}(x,y,z) = \sqrt{\left(x - x_{i,j}\right)^2 + \left(y - y_{i,j}\right)^2 + z^2} \qquad 3$$

For isotropic materials the velocity profile is constant whereas for the corrected imaging of single crystals the anisotropic velocity profile must be used. In the single crystal case the orientation of the crystal within each specimen affects the anisotropic velocity profile. Therefore, the crystallographic orientation of each specimen must be measured prior to inspection to implement the algorithm.

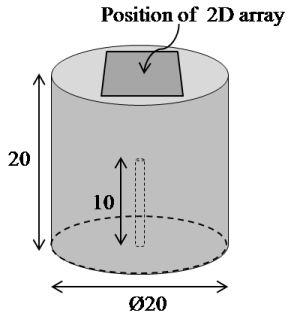

Figure 4. Diagram of test piece with a 1 mm diameter spherical-ended hole drilled from the centre of one of the flat surfaces. All measurements are in mm.

To demonstrate the effect of using the correct algorithm for ultrasonic image reconstruction, array data from isotropic and single crystal test specimens were collected. The specimen, shown in Figure 4, was a 20 mm diameter, 20 mm long cylinder containing a 1 mm diameter spherical-ended hole drilled from the centre of one of the flat surfaces. The isotropic test piece was manufactured from an equiaxed nickel alloy with a constant longitudinal velocity of 6060 m/s and the single crystal test piece was cast from CMSX-4. The single crystal test specimen was cast approximately in the [001] direction. The actual crystallographic orientation was found using a Laué X-ray diffraction method detailed in Jones et al [(9)] which has an orientation accuracy of $\pm 0.8^0$. The specimens were inspected with a 12x6 element 10 MHz 2D array with a 0.6 mm element pitch manufactured by Sonaxis, Besançon France, using a Micropulse MP5PA array controller from Peak NDT Ltd, Derby UK.

The 3D TFM algorithm was run on both sets of data. In the anisotropic case, the data was first processed with constant velocity then the corrected algorithm was implemented that used the modelled velocity profile. In this example the array image was constructed using the longitudinal mode and hence the bulk longitudinal velocity profile of CMSX-4, as shown in Figure 2, was used.

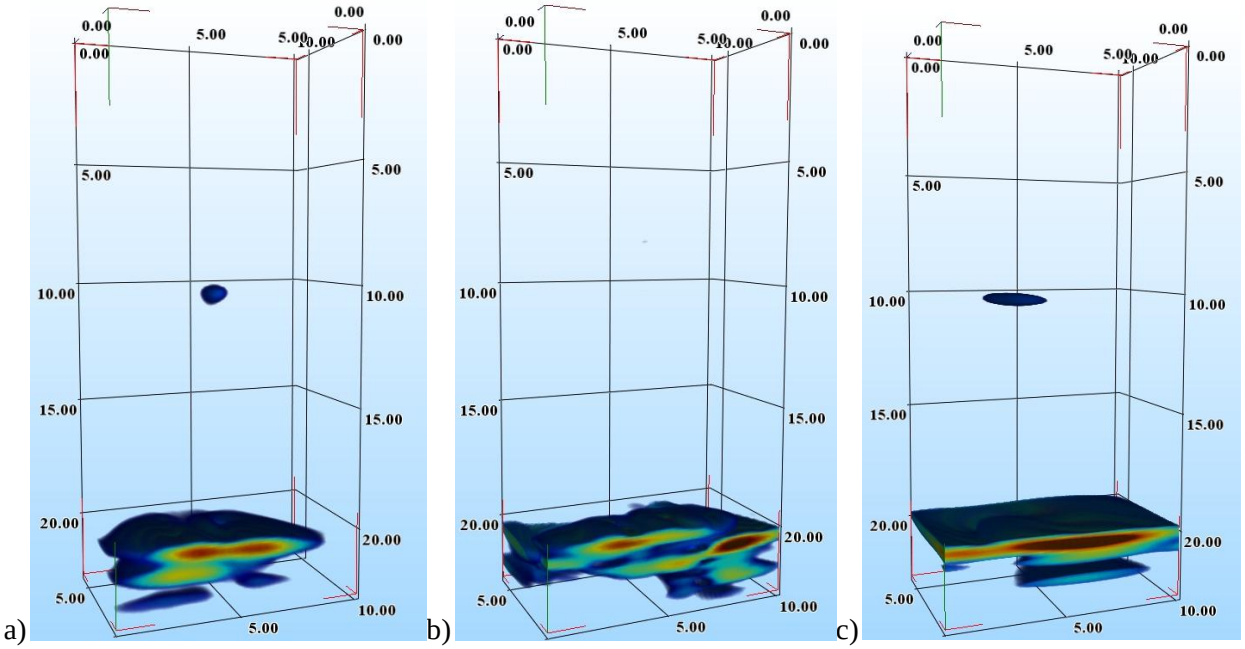

Figure 5. 3D TFM images from experimental data for a) isotropic, b) uncorrected anisotropic and c) corrected anisotropic materials. The images are displayed by rendering all isosurfaces 24 dB below the peak back wall signal of each image.

Figure 5 shows the TFM images of the isotropic test piece and the uncorrected and corrected images for the anisotropic single crystal test piece. The defocusing effect of the anisotropy can be seen to cause significant distortion in the uncorrected image which does not display an indication from the spherical-ended hole. Once the corrected algorithm is applied, the spherical-ended hole is imaged as a point-like reflector at x = 10 mm and the back wall is displayed as a flat surface correlating closely with the isotropic image.

Inspection of a Single Crystal Turbine Blade

The corrected ultrasonic imaging algorithm was then applied to a typical turbine blade cast from single crystal CMSX-4. The blade under inspection contained a through-going 3 mm long slot in its root section which simulated a crack-like defect. The root section of the blade is one of the most highly stressed regions and so it is possible cracks could initiate from this location, hence the desire to inspect this area in particular.

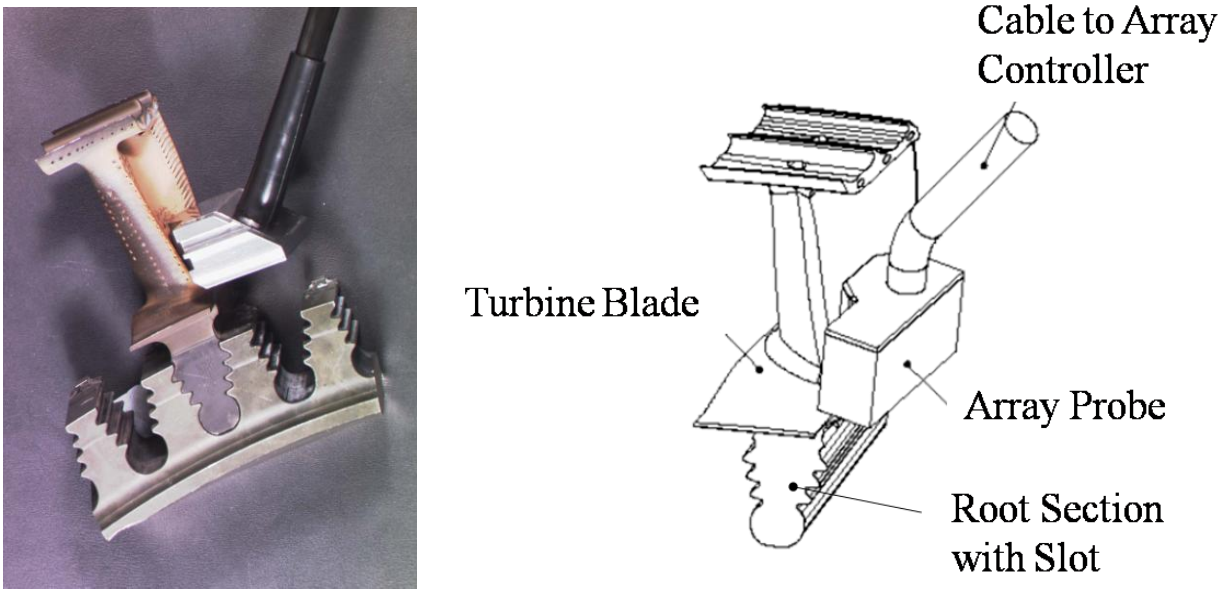

Figure 6. Images of the 2D ultrasonic array probe on the turbine blade. Image courtesy of Sonaxis.

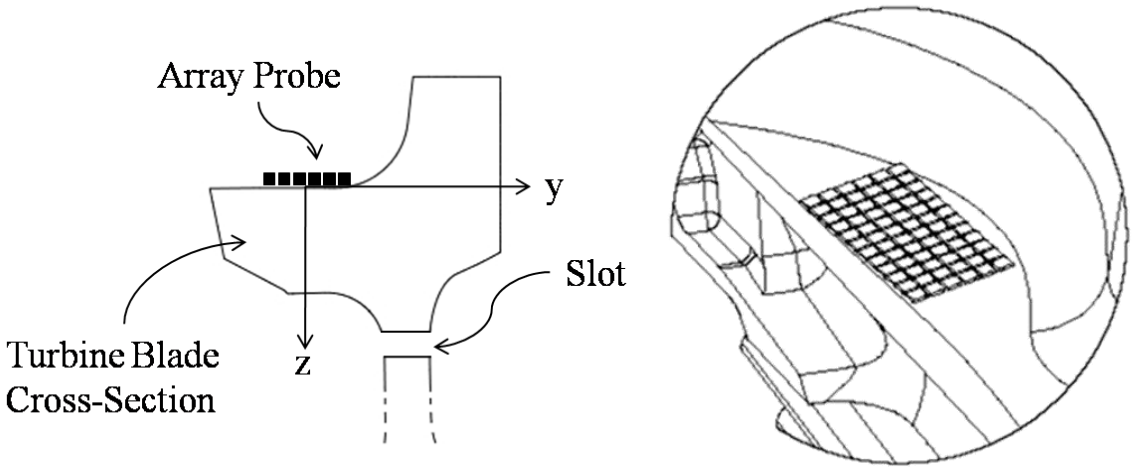

Figure 7. Schematic diagram of the ultrasonic array on a turbine blade with a root slot.

Figure 6 shows images of the 10 MHz array probe placed on the exterior of the turbine blade positioned to inspect for the machined slot. Figure 7 is a schematic diagram of this configuration and shows how the position of the array elements relates to the root slot.

The FMC data from the 10 MHz array probe was captured on the blade platform using the array controller. The crystallographic orientation of the blade was measured using X-ray diffraction then the corrected algorithm was run on the data. Figure 8 shows the reconstructed TFM image of the turbine blade with 3 mm slot. The back wall of the blade platform and the slot can be clearly seen in the volumetric image showing that the inspection system has been implemented successfully.

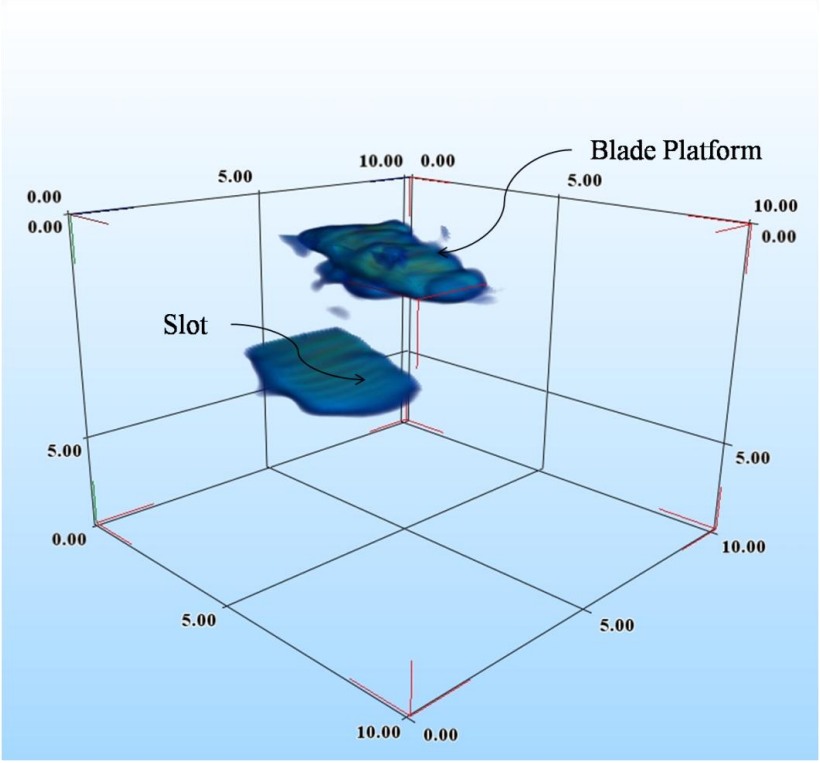

Figure 8. Corrected TFM image of the slotted turbine blade root. The images are displayed by rendering all isosurfaces 24 dB below the peak blade platform signal.

Conclusions

This paper has shown that ultrasonic array images may be corrected to account of the anisotropic nature of single crystal components by using modelled velocity profiles. These methods have been applied to a typical single crystal turbine blade with a simulated defect. It has been shown that the using the developed algorithm, the slot within the turbine blade root can be successfully detected.

For the corrected algorithm to be implemented, the crystallographic orientation of the specimen must be known. This was achieved in this paper using X-ray diffraction methods that are frequently used for single crystal castings. However if the 2D array system is to be deployed for *in-situ* inspections, which removes the costly process of dismantling the engine, X-ray diffraction cannot be used due to size and access constraints. Therefore, an ultrasonic method that uses the same 2D array that performs the NDT inspection to first measure the crystallographic orientation will be investigated.

References

1. **Mondal, S, Wilcox, P D and Drinkwater, B W.** Design of Two-Dimensional Ultrasonic Phased Array Transducers. *Journal of Pressure Vessel Technology.* 2005, Vol. 127, pp. 336-344.

2. **Frasier, D, et al.** Process and Alloy Optimization for CMSX-4 Superalloy Single Crystal Airfoils. *High Temperature Materials for Power Engineering.* 1990, pp. 1281-1300.

3. **Lane, C J L, et al.** 3D ultrasonic inspection of anisotropic aerospace components. *Insight.* February 2010, Vol. 52, No 2.

4. **Musgrave, M. J. P.** *Crystal Acoustics.* Cambridge : Cambridge Unvierstiy Press, 2001.

5. **Červený, V.** *Seismic Ray Theory.* Cambridge : Cambridge University Press, 2001. ISBN 0 521 36671 2.

6. **Rose, J L.** *Ultrasonic Waves in Solid Media.* Cambridge : Cambridge University Press, 1999. ISN 0 521 54889 6.

7. **Auld, B A.** *Acoustic Fields and Waves in Solids. Volume 1.* New York : John Wiley & Sons, Inc, 1973.

8. **Wilcox, P D, Holmes, C and Drinkwater, B W.** Advanced Reflector Characterization with Ultrasonic Phased Arrays in NDE Applications. *IEEE Transactions on Ultrasonics, Ferroelectrics, and Frequency Control.* August 2007, Vol. 52, No 2.

9. **Jones, A and Baxter, C.** The Rolls-Royce Scorpio System. *Measurement Science and Technology.* 1995, Vol. 6, pp. 131-133.